Exploring the Relationship between Geothermal Resources and Geodetically Inferred Faults Slip Rates in the Great Basin

William C. Hammond, Corné Kreemer, Geoff Blewitt

Nevada Bureau of Mines and Geology and Seismological Laboratory
University of Nevada, Reno

ABSTRACT

We present the results of GPS measurement and modeling of active crustal deformation and its spatial relationship to active geothermal systems in the northern Walker Lane. Using a block modeling method we use the GPS data to estimate the slip rate and style on faults in our study area. Our results show that there is a spatial correlation between zones of high dextral slip rate that also have a component of normal slip and the presence of geothermal systems. This is consistent with earlier work that showed a correlation between regional transtensional areal strain and the presence of geothermal systems, but goes further by combining the GPS data with structural data on fault surface trace geometries. Before block modeling we apply a correction for postseismic relaxation following the historic earthquakes of the Central Nevada Seismic Belt. We find that in a few localities the relaxation-corrected GPS velocity field is in conflict with geologic data, indicating that the MAGNET data are providing additional constraints that improve our understanding of the transient postseismic response, and will be incorporated in future models.

Introduction

Geothermal energy resources have long been associated with the presence of crack systems that are presumed to provide pathways for transport of hot fluids. It has been shown in a few recent studies that productive non-magmatic geothermal systems in the western Great Basin exhibit a correlation with active tectonic deformation [e.g. *Faulds et al.*, 2005] and the presence of nearby fault systems [e.g. Goranson and van de Camp, 2005]. Based on data obtained with the Global Positioning System (GPS), it was concluded by *Blewitt et al.*, [2002, 2005] that regional patterns of geodetically measured transtensional strain are also strongly correlated with the presence of hydrothermal output. It was hypothesized that the mechanisms behind this correlation were likely associated with the regional transtensional interseismic strain accumulation imposing a state of stress that promotes the opening of cracks or pore spaces near the fault to allow fluid transport. Beyond this general observation, understanding the physics behind the relationship between geothermal resources and tectonics remain enigmatic. A key question that remains to be satisfactorily answered is: Which is more important for providing the conditions necessary to develop active hydrothermal output, the crustal deformation rate or slip style, or both?

We address this question by using geodetic measurements to constrain the rate and style of slip on the faults in our study area (Figure 1). We interpret the GPS velocity field using a block modeling methodology that estimates the direction of motion and rotation of crustal blocks with respect to one another. This technique is a compliment to areal strain rate methods (e.g. *Kreemer et*

al., 2006) that models the crust essentially as an unbroken continuum. Which description is preferable (continuum vs. blocks) depends on the investigator's objectives, spatial scale of interest, and time of observation with respect to the earthquake cycle. In the northern Walker Lane and western Great Basin crustal faulting is pervasive, and hence there are many crustal blocks (Figure 1) whose lateral dimensions are similar to the depth of locking of block bounding crustal faults. A result of this is that the GPS velocity across our network in the interseismic (between large earthquakes) time varies smoothly. Thus the deformation behavior of northern Walker Lane lies in a realm of transition between large rigid entities (e.g. plates) and smoothly deforming continuum (e.g. a fluid). Here we use a block approach to attempt to isolate which faults systems are most active, and investigate whether the related deformation pattern is an important control on the generation of geothermal resources.

MAGNET GPS Network

Installation of the Mobile Array of GPS for Nevada Transtension (MAGNET) began in January 2004. Since that time 146 stations have been installed in a part of the western Basin and Range, Walker Lane Belt and Central Nevada Seismic Belt delineated approximately by the area shown in (Figure 1). The network occupation schedule is termed "semi-continuous", which is a style of measurement that is a hybrid between continuously recording, permanently fixed GPS receivers and campaign GPS, which are occupied episodically (e.g. yearly) with temporary monumentation such as tripods. Continuous GPS is far more accurate than campaign GPS because of superior stability and greater amount of data collected. We have found that the semi-continuous methodology used in MAGNET is an excellent compromise between the stability and measurement repeatability of continuous GPS and the spatial coverage of campaign GPS for an overall increase in efficiency of sampling of the surface deformation field [*Blewitt et al.*, 2007]. This study area also contains 12 continuous GPS receivers from the Basin And Range GEodetic Network (BARGEN – *Wernicke et al.*, 2000) and Plate Boundary Observatory (PBO) GPS networks whose data we also include in our analysis. Furthermore, we have included data obtained during USGS campaigns in the area from the studies of [*Svarc et al.*, 2002; *Hammond and Thatcher*, 2004; *Hammond and Thatcher*, 2007].

GPS Velocity Analysis

We used GPS data up to April 21, 2007, obtaining for each site daily estimates of position coordinates with the GIPSY/OASIS II software package from the Jet Propulsion Laboratory in precise-point-positioning mode with carrier phase ambiguities resolved (bias-fixed) [*Blewitt et al.,* 1989; *Zumberge et al.*, 1997]. Sites with less than one year of data spanned by their time series were not considered since their velocity estimates are too uncertain to be useful for estimating strain patterns in the Walker Lane. To eliminate sources of noise present in GPS time series that come from global uncertainty in reference frame we apply a spatial filtering algorithm to the time series using linear, annual and semi-annual terms that improves our estimates of regional secular strain. The BARGEN sites SHIN, QUIN, GARL, TUNG, GABB, NEWS, MONI were used as reference stations for this filtering since they run continuously and provide a stable reference. For the continuous sites we only included data after January 1, 2000 owing to systematic antenna equipment changes near the end of 1999 which can cause discontinuities in the time series. Site velocities are obtained from a regression of the residual time series and then the solution is rotated so that

velocities refer to a fixed North America Reference. For the velocities shown in Figure 1, we subtracted the average velocity between longitude 117.3W and 117.0W to emphasize the changes in velocity across the network.

After the above criteria have been applied there are 58 MAGNET velocities, 13 continuous site velocities and 61 campaign GPS velocities inside the study area, for a total of 132 GPS velocities (Figure 1). A few sites exhibit velocities that are clearly anomalous with respect to the regional pattern. For this reason we did not include the sites HONY, RATT, or KINS in our block modeling because their azimuths deviate substantially from the regional pattern. Many of the campaign GPS velocities appear to have anomalous azimuths as well, but their uncertainties are so much greater that these perturbations have little effect on the final model.

Postseismic Relaxation

In the 20th century a belt-like sequence of large (M>6.5) earthquakes occurred in central Nevada (Bell et al, 2005). Stress changes from these Central Nevada Seismic Belt (CNSB) earthquakes appear to have induced a transient postseismic relaxation response in the lower crust and upper mantle which is characteristic of viscoelastic rheology of the lithosphere [*Hetland and Hager*, 2003; *Gourmelen and Amelung*, 2005; *Hammond et al.,* 2007]. The magnitude of this response is on the order of a few mm/yr across the CNSB and has a strong effect on the interpretation of the modern GPS velocity field in terms of secular strain accumulation on faults. To separate strain accumulation (which is related to the long-term loading of faults) from the transient relaxation (which fades to zero over time) we have modeled the response of the earthquakes using the regional campaign and continuous GPS velocities. However, this modeling was necessarily completed before MAGNET velocities, which are superior in precision and spatial coverage, were available. Our results, discussed below, reveal some shortcomings of the first-generation postseismic modeling that will be eliminated when we redo the modeling including the new MAGNET data. To illustrate the effect of this correction we show the velocity field with and without the correction (Figures 1b and 1c), but used the corrected velocity field in the block modeling.

Block Modeling

Block modeling is advantageous in studies of crustal deformation because it allows integration of geodetic data with the geometry of fault surface traces and fault slip style. In this context blocks are essentially units of lithosphere that are completely bounded by faults so that they may move as rigid elements with respect to other blocks. Our formulation [*Hammond and Thatcher*, 2007] is similar to other block modeling strategies [e.g. *McCaffrey*, 2002; *Meade and Hagar*, 2005] and accounts for the deformation that is observed at the surface near faults during the interseismic time frame. During this time the faults that bound the blocks are locked at the surface and do not slip. It is important to account for this so that all GPS velocities drive block motion, regardless of their proximity to faults. Because we estimate the long term motion of the blocks (over many seismic cycles) the model also provides estimates of the relative motion between blocks, i.e. slip rates on the bounding faults.

Our model (Figure 1b) has 62 blocks and 221 fault segments that follow the traces of active faults obtained from several databases including the USGS Quaternary Fault and Fold Database [*Cao et al.,* 2003; *Haller et al.* 2002]. Strike slip faults dip 90° and normal faults dip 45° in the direction of hanging wall. All faults are locked from the surface to a depth of 15 km, (i.e. are not allowed to "creep") in accordance with the depth of most crustal seismicity in the Basin and Range. All blocks move freely according to the GPS data except for the Sierra Nevada block (lower leftmost block in Figures 1 and 2), which was constrained to move with the entire rigid Sierra Nevada/Great Valley microplate according to 6 continuous GPS receivers distributed near the center of the microplate.

Because the number of blocks is about half the number of GPS data, the model is underdetermined in some regions. The southern part of our study area in particular has many sites that have been only recently installed, and thus do not yet have over 1 year of data and thus were not included in our analysis. We present here a model that is strongly damped, i.e. estimating minimum slip rates on all fault systems that result in a model that explains the data as well as the best fitting model (Figure 2). This method is preferable to using a model with fewer blocks because we do not have to specifiy *apriori* the location of the most active faults. This strategy tends to find features in the model that are required by the data, and not simply allowed by the data. In this model we therefore image no deformation where there is insufficient geodetic data to form velocities (e.g. near 38.5°N between -119.2°W and 118.3°W) except where such deformation is required to conform to the block modeling assumptions of regional kinematic consistency, and as driven by data elsewhere in the model.

Formal uncertainties in GPS inferred positions found using GIPSY/OASIS II software are often found to be unrealistically small. We found that the normalized residual RMS misfit of our block model was ~4.0. One possibility is that the uncertainty in our velocities should be scaled by this factor. The uncertainties in Figure 3 have this scaling applied.

Results and Discussion

The estimates of slip rate are shown in Figure 2. The motion is predominantly dextral slip with normal slip isolated focused into three specific areas. The highest dextral and normal slip rates in the model occur near the westernmost faults bounding the Sierra Nevada/Great Valley microplate. The faults in the vicinity of Lake Tahoe appear to be accommodating the most normal slip. This is consistent with the profile of GPS velocity which is steepest (highest strain rate) at the west side of the network (Figure 3). The Mohawk Valley fault system in Northern California is the fastest slipping at a dextral rate of 3.9 mm/yr. The next most prominent feature in the model is the high dextral slip occurring along a system connecting the Petrified Springs/Benton Springs faults east of Walker Lake, passing northwestward through the Carson Sink and connecting to the Pyramid Lake fault. This northwest trending dextral slipping fault has a rate of 1.6 to 2.1 mm/yr. The apparent rigidity of the crust between this system and the Tahoe system of faults, however, may be owing to the fact that we have few model constraints here (Figure 1c).

Two other zones of crustal extension are present in the model. First, the Dixie Valley Stillwater faults were the locus of two of the CNSB earthquakes in 1954. The model has extension rates of 0.3 to 0.5 mm/yr (projected to the horizontal) for Dixie Valley and 0.5 mm/yr for Stillwater

fault, giving a sum of rates near 1 mm/yr, similar the results of paleoseismic studies of CNSB faults [*Bell et al.,* 2004]. Second, we see combined east-west extension rate of ~1.4 mm/yr in the vicinity of the faults both west and east of the Granite Springs Valley.

It is important to recognize the limits of the resolution of our modeling. Because the faults are locked at the surface the geodetic velocity signal from any given fault is spatially smoothed at the surface, implying that slip from one fault could be imaged onto a nearby fault if it is closer than the fault locking depth. For example, while the model shows the fastest normal slip rates on the west side of Lake Tahoe, some of this slip could actually be occurring on faults immediately east of the Tahoe Basin without a significant change in data misfit. Planned future developments in our modeling abilities will allow us to express this model covariance more precisely. What is robust is the sum of slip rates over clusters of nearby faults, so for the Tahoe example it is likely that the set of faults (e.g. Genoa, Tahoe Basin, east Carson Valley faults) are together accommodating more slip than faults elsewhere in the Walker Lane.

There are a few instances of where the model indicates a thrust sense motion on faults, the most significant of which is the northern edge of the Carson Sink. Comparison of Figures 1b and 1c indicates that the convergence between the adjacent blocks is not present before the correction for postseismic relaxation is made. A constraint in the postseismic modeling was applied that created misfit if contraction was inferred from the corrected GPS velocities, but this constraint was applied on regional averages over hundreds of km, and not on the scale of individual faults that we model here. Thus the new MAGNET GPS data and our modeling have revealed what is likely a shortcoming in the details of the postseismic model. This feature will be corrected once we use MAGNET data to constrain the models of postseismic relaxation.

There appears to be a spatial correlation between the high rates of dextral slip passing through the Carson Sink and the relative abundance of geothermal resources there. In fact, most of the sites in our study area with geothermal resources lie within 30 km of the dominant zones of right lateral slip through the Walker Lane. The majority of these systems, i.e. in the Carson Sink, Honey Lake and Pyramid Lake localities lie near dextral slip faults that exhibit a small component of normal extensional motion. These findings are consistent with previous work [*Blewitt et al,* 2002;2005, *Kreemer et al.,* 2006] and show that there is a clear trend for geothermal systems to be preferentially located in parts of the Basin and Range that exhibit transtensional crustal deformation. The lack of geothermal systems near the Mohawk fault zone is and example of how a high dextral slip rate is not a sufficient criterion to predict the presence of geothermal resources. The component of normal extension is required. Note that the faults in the vicinity of Pyramid and Honey lakes do have a component of normal slip, but they are not plotted because the rates are not significantly greater than zero, a condition that may change once we have continued our data collection and reduced GPS velocity uncertainties further.

Acknowledgments

References

Bell, J. W., S. J. Caskey, A. R. Ramelli, and L. Guerrieri, 2004, Pattern and rates of faulting in the central Nevada seismic belt, and paleoseismic evidence for prior belt-like behavior, Bull. Seismol. Soc. Am., 94, 1229-1254.

Blewitt, G., 1989, Carrier phase ambiguity resolution for the Global Positioning System applied to geodetic baselines up to 2000 km, J. Geophys. Res., 94, 10,187-110,283.

Blewitt, G., M. Coolbaugh, W. E. Holt, C. Kreemer, J. L. Davis, and R. A. Bennett, 2002, Targeting of Potential Geothermal Resources in the Great Basin from Regional Relationships between Geodetic Strain and Geological Structures, Transactions Geothermal Resources Council, 26, 523-526.

Blewitt, G., W. C. Hammond, and C. Kreemer, 2005, Relating geothermal resources to Great Basin Tectonics using GPS, Geothermal Resource Council Transactions, 29, 331-335.

Blewitt, G., W. C. Hammond, and C. Kreemer, 2007, Geodetic constraints on contemporary deformation in the northern Walker Lane: 1, Semi-permanent GPS strategy, in Late Cenozoic Structure and Evolution of the Great Basin – Sierra Nevada Transition, edited by J. S. Oldow and P. Cashman, Geological Society of America.

Cao, T., W. A. Bryant, B. Rowshandel, D. Branum, and C. J. Wills, 2003, The revised 2002 California probabilistic seismic hazard maps, California Geological Survey.

Davatzes, N. C., and S. H. Hickman, 2005, Controls on fault-hosted fluid flow: Preliminary Results from the Coso Geothermal field, CA, Geothermal Resource Council Transactions, v 29.

Faulds, J. E., C. D. Henry, M. Coolbaugh, and L. H. Garside, 2005, Influence of the late Cenozoic Strain field and tectonic setting on Geothermal activity and mineralization in the northwestern Great Basin, Geothermal Resource Council Transactions, 29, 353-358.

Gourmelen, N., and F. Amelung, 2005, Post-seismic deformation in the central Nevada seismic belt detected by InSAR: Implications for Basin and Range dynamics, Science, 310, 1473-1476.

Haller, K. M., R. L. Wheeler, and K. S. Rukstales (2002), Documentation of changes in fault parameters for the 2002 National Seismic Hazard Maps - Conterminous United States except California, 34 pp, U.S. Geological Survey.

Hammond, W. C., and W. Thatcher, 2004, Contemporary tectonic deformation of the Basin and Range province, western United States: 10 years of observation with the Global Positioning System, J. Geophys. Res., 109, B08403, doi:10.1029/2003JB002746.

Hammond, W. C., and W. Thatcher, 2007, Crustal Deformation across the Sierra Nevada, Northern Walker Lane, Basin and Range Transition, western United States Measured with GPS, 2000-2004, J. Geophys. Res., 112.

Hammond, W. C., C. Kreemer, and G. Blewitt, 2007, Geodetic constraints on contemporary deformation in the northern Walker Lane: 3, Postseismic relaxation in the Central Nevada Seismic Belt, Late Cenozoic Structure and Evolution of the Great Basin – Sierra Nevada Transition.

Hetland, E. A., and B. H. Hager, 2003, Postseismic relaxation across the Central Nevada Seismic Belt, J. Geophys. Res., 108, 2394, doi:10.1029/2002JB002257.

Goranson, C., and P. van de Kamp, 2005, Geologic Structure of the Hot Sulpher Springs Geothermal area, Tuscarora, Nevada, Geothermal Resource Council Transactions, 29, 359-362.

Kreemer, C., G. Blewitt, and W. C. Hammond, 2006, Using geodesy to Explore Correlations between crustal deformation characteristics and geothermal resources, Geothermal Resource Council Transactions, 30, 441-446.

McCaffrey, R., 2002, Crustal block rotations and plate coupling, 101-122 pp., AGU Geodynamics Series v. 30, edited by S. Stein and J. Freymueller.

Meade, B. J., and B. H. Hagar, 2005, Block models of crustal motion in southern California constrained by GPS measurements, J. Geophys. Res., 110.

Svarc, J. L., J. C. Savage, W. H. Prescott, and A. R. Ramelli, 2002, Strain accumulation and rotation in western Nevada, 1993-2000, J. Geophys. Res., 107, 10.1029/2001JB000579.

Wernicke, B. P., A. M. Friedrich, N. A. Niemi, R. A. Bennett, and J. L. Davis, 2000, Dynamics of plate boundary fault systems from Basin and Range Geodetic Network (BARGEN) and Geologic Data, GSA Today, 10, 1-7.

Zumberge, J. F., M. B. Heflin, D. C. Jefferson, M. M. Watkins, and F. H. Webb, 1997, Precise point positioning for the efficient and robust analysis of GPS data from large networks, J. Geophys. Res., 102, 5005-5017.

Figure 1 a) Study area with topography, active faults (black lines), geothermal power plants (large yellow triangles), and hydrothermal systems >150 C (small yellow triangles) , b) block boundaries and GPS velocities from MAGNET (red), regional continuous sites (black), and campaign sites (green) with respect to easternmost side of the area. Ellipses around tips of vectors denote uncertainties at 95% confidence, (where they appear missing they are too small to see). c) same velocities but corrected for the effects of CNSB postseismic relaxation according to the model of *Hammond et al.*, [2007].
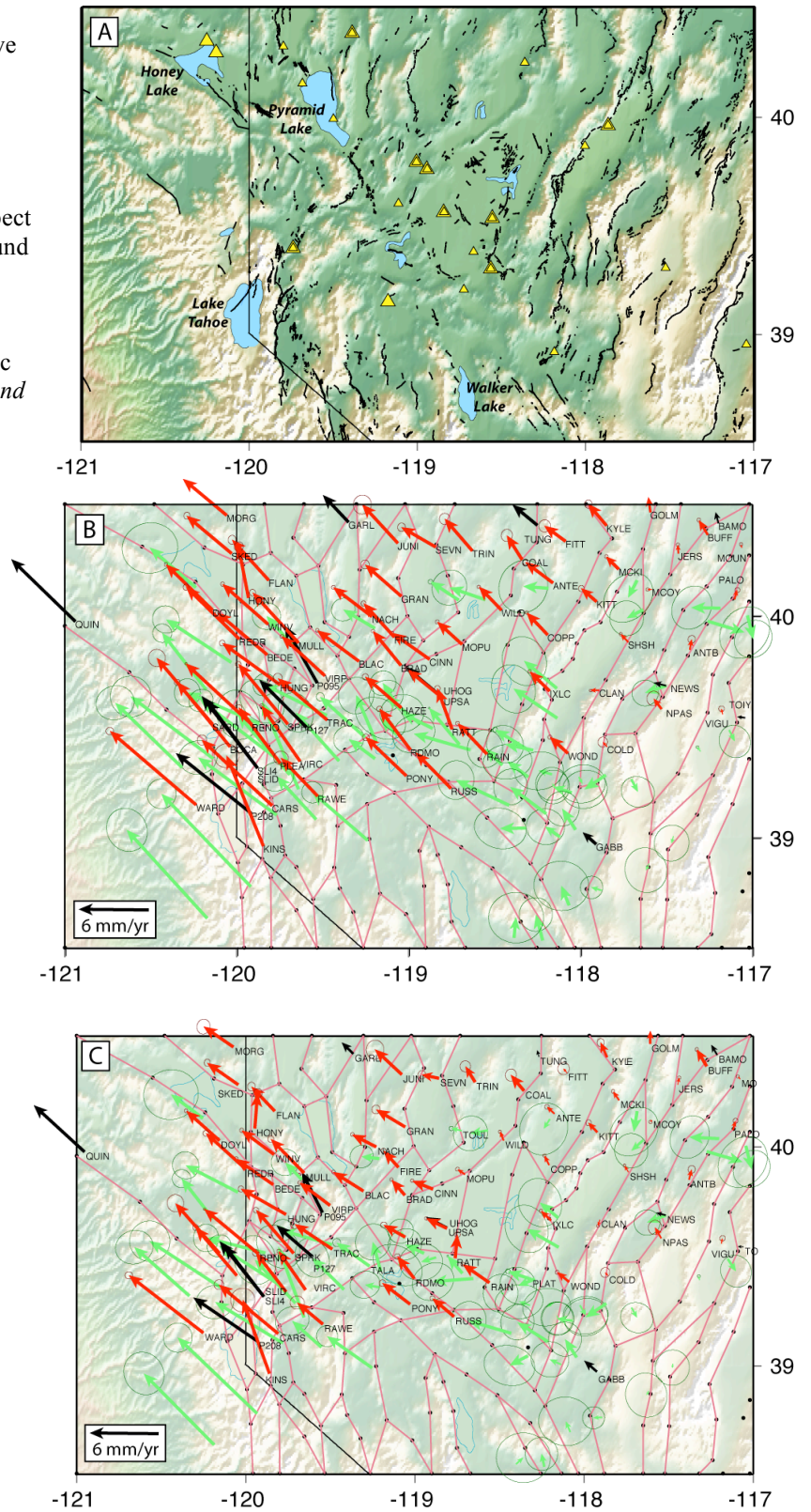
Figure 2. Same as Figure 1a except with slip rates on faults inferred from GPS velocities. Black (red) lines indicate dextral (sinistral) slip, with line thickness indicating rate. Blue (cyan) segment crossing a fault indicates normal (reverse) slip with length indicating rate. Only slip rates that are within 95% confidence significantly different from zero are shown.
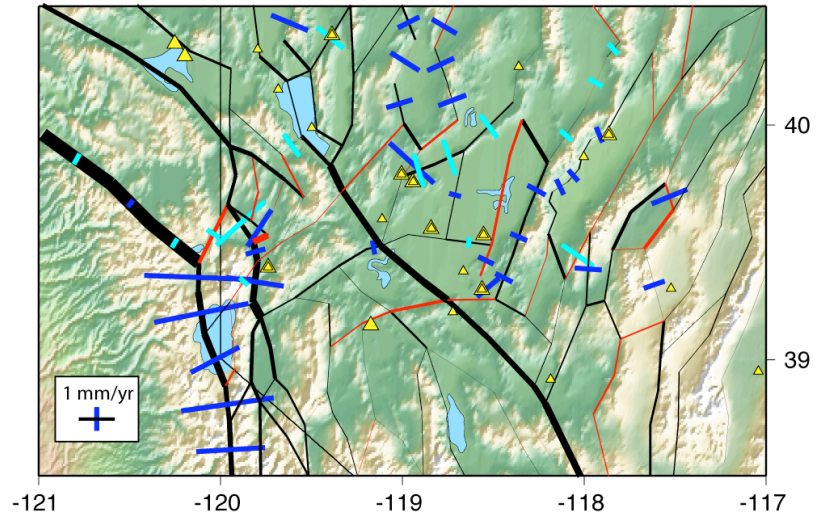

Figure 3. Magnitude of GPS velocity with respect to stable North America across east-west profiles for a) north profile (sites between 39.75°N and 40.5°N latitude), b) south profile (between 38.5°N to 39.75°N). GPS velocities (blue dots) have been corrected for postseismic relaxation from CNSB earthquakes, and are shown with the scaled 2-sigma uncertainty bars. Open triangles are the velocity predicted from the block model shown in Figure 2. Campaign GPS velocities are not shown to improve clarity.